SCIENTIFIC REPORTS

OPEN

SUBJECT AREAS:
FUEL CELLS
SURFACE SPECTROSCOPY
ELECTROCATALYSIS
CHARACTERIZATION AND ANALYTICAL TECHNIQUES

Received
22 March 2013

Accepted
16 August 2013

Published
4 October 2013

Correspondence and requests for materials should be addressed to B.B. (benedetto.bozzini@unisalento.it) or M.K. (maya.kiskinova@elettra.trieste.it)

In-situ Photoelectron Microspectroscopy and Imaging of Electrochemical Processes at the Electrodes of a Self-driven Cell

Benedetto Bozzini[1], Matteo Amati[2], Luca Gregoratti[2] & Maya Kiskinova[2]

[1]Dipartimento di Ingegneria dell'Innovazione, Università del Salento, via Monteroni, 73100 Lecce – Italy, [2]Elettra-Sinctrotrone Trieste S.C.p.A., S.S. 14, km 163.5 in Area Science Park, 34149 Trieste-Basovizza – Italy.

The challenges in development of solid oxide fuel cells (SOFCs) are reducing their dimensions and increasing their efficiency and durability, which requires physicochemical characterization at micro-scales of the device components during operation conditions. Recently, the unique potential of scanning photoelectron microscopy (SPEM) has been demonstrated by in-situ studies of externally-driven SOFCs, which mimic real devices. Here we overcome the gap between model and real systems using a single-chamber Ni|YSZ|Mn SOFC, supporting a range of self-driven electrochemical reactions in variable gas environments and temperatures. The reported SPEM results, obtained during spontaneous electrochemical processes occurring in reactive gas ambient, demonstrate the chemical evolution of electrodic material, in particular the lateral distribution of the oxidation state and the induced local potential, clearly marking out the electrochemically most active micro-regions of the Ni anode.

Electrochemistry is strongly contributing to the current energetic agenda aiming at efficient, renewable and eco-sustainable generation, conversion and storage of electrical energy. Although the mechanisms of energy conversion and storage are different, a common feature in devices such as fuel cells, batteries, ultracapacitors and photoelectrochemical cells is that all important processes occur at the electrode/electrolyte interface. Indeed, the most commonly used current–voltage (I–V) characteristics provide information about the overall electrochemical reaction, but for improving the electrode efficiency and impeding degradation processes, correlative knowledge about the status of electrode surface under realistic operating conditions is of fundamental importance. In this respect, photoelectron spectroscopy (PES) has long been recognized as a powerful tool for understanding and solving important issues relevant to operation of electrochemical devices, where the performance is strongly dependent on the electrode surface status[1]. The recent in-situ photoelectron spectroscopy (PES) studies of model SOFCs with lateral resolution ranging from few tens of μm[2,3], to a sub-μm[4–7], have provided a wealth of information about the electrochemical, mass transport and side processes occurring in operating devices. Chiefly, due to experimental difficulties, the electrodic reactions in these studies were driven by an external power source using proper polarization levels. In brief, the obtained results have revealed the evolution of the electrode chemical state and electrochemical activity across the electrode/electrolyte interfaces, as well as the occurrence of undesired irreversible processes reducing the durability of the device components, such as temperature- and potential-promoted changes in the electrode microstructure and corrosion, mass transport of interconnect and electrode constituents and deposition of contaminants. Unfortunately, in such model externally-driven systems the coupling between the anodic and cathodic phenomena, which plays a crucial role in the real self-driven cells in terms of efficiency and durability, are intrinsically excluded. This inspired the present '*under operando*' investigation with a *self-driven* cell, where the potentials at the electrodes are natural consequence of electric current generated by electrochemical processes controlled by the gas (H_2 or H_2 + O_2) reactant ambient. Relevant to the present study, but both methodologically and experimentally different as an approach, is the reported evolution of the oxidation states of Ni electrodes in *externally*-driven SOFCs. In these studies reversible oxidation-reduction processes were induced independently of the gas ambient only by changing the sign of the applied bias[5,6,8].

Results

Following our proof-of-principle scanning photoelectron microscopy (SPEM) experiments with a single-chamber SOFCs using a $CH_4 + O_2$ mixture[9], here we report the first in-situ SPEM study of a self-driven device system monitoring simultaneously the chemical state and local potential at the electrodes during spontaneous conversion of the chemical into electrical energy. The used planar single-chamber cells, sketched in Figure 1 (a) consist of Mn cathode and Ni anode deposited on a YSZ(110) electrolyte. By pre-exposing the cell to H_2 and O_2 it was possible to form different redox electrode couples (Ni/NiO and MnO/MnO_2) giving rise to the generation of electrical power. Details on the cell fabrication, material combinations and corresponding thermodynamics are provided in SI. It is worth noting that the details of the material combinations expounded in Section 2 of SI can yield either steady-state or transient self-driven behaviour.

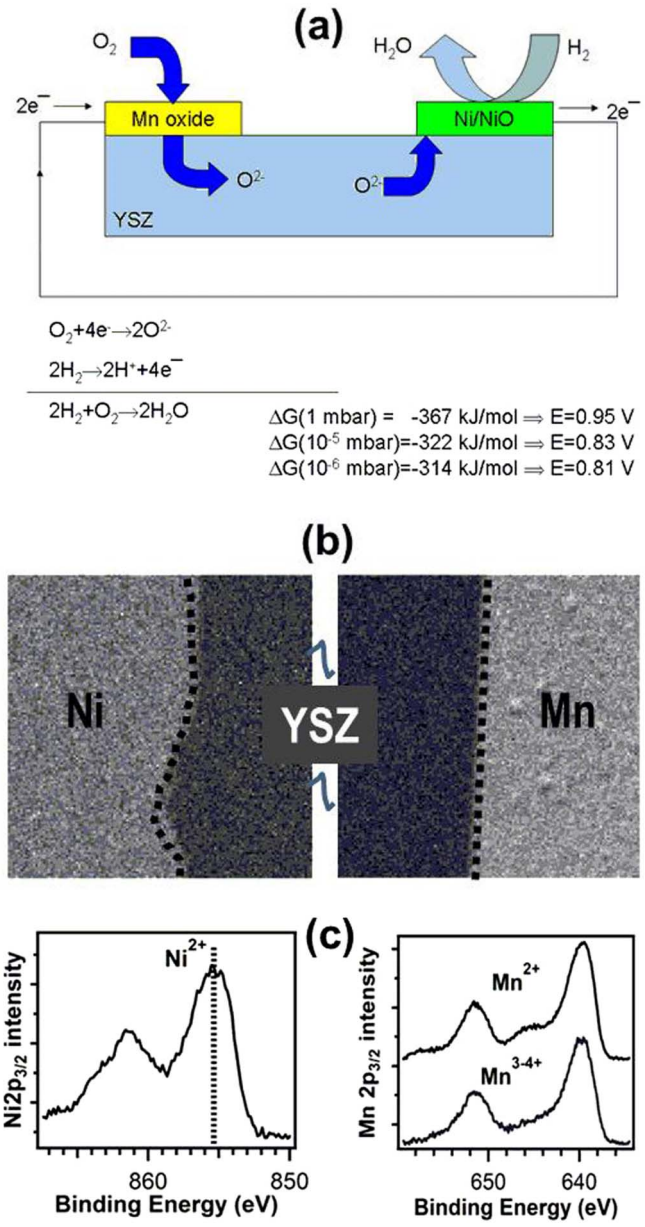

Figure 1 | (a) Scheme of the planar cell for in-situ electrochemical SPEM measurements. (b) Ni $2p_{2/3}$ and Mn 2p SPEM images (128 × 128 μm²) of the pristine cell (650°C): bright areas with sharp edges correspond to the Ni and Mn electrodes and the dark ones to the YSZ electrolyte. The dark dots close to the electrode edge indicate the most active region (c) Ni $2p_{2/3}$ and Mn 2p (bottom spectrum in Mn panel) μ-PES of the cell electrodes before starting the reaction (650°C). The top spectrum in the Mn panel corresponds to the partially reduced Mn state.

The cells were run at 650°C by alternative feeding with fuel (H_2) and oxidant (O_2) or with fuel and oxidant ($H_2 + O_2$) mixture. The dynamics of H_2 electrochemical oxidation during self-driven cell operation was followed using both imaging and μ-PES modes, namely mapping the evolution of selected regions tuning the analyser to the energy window of a selected core level spectrum or recording high resolution Ni 2p and Mn 2p spectra from micro-spots, representing the most active zones close to the electrode/electrolyte interface or other areas of interest. Since the kinetic energies of emitted photoelectrons are also sensitive to the local potential, along with chemical shifts, the photoelectron spectra can undergo a rigid overpotential energy shift[2,3,6,7] that we use for monitoring the onset of current flow in the cell.

From all possible types of electrochemically self-driven systems, described in the SI, we report here the results on two representative ones: (i) MnO_2 cathode/YSZ/NiO anode run in anodically reactive H_2 and (ii) MnO_2 cathode/YSZ/NiO anode run in cathodically and anodically reactive $H_2 + O_2$ mixture. The cell was short-circuited through a potentiostat working in a ZRA (zero-resistance ammetry) mode for simultaneous monitoring of the current response. Results for other two cases: (i) termination of the electrochemical reaction by switching the operation from H_2 to O_2 ambient and (ii) termination of H_2 reduction by switching from H_2 to UHV ambient are reported in the SI.

The grainy morphology of the Mn and Ni electrodes attained when exposed to O_2 atmosphere at 650°C before switching the gas ambient for starting the electrochemical reaction, is exemplified by the Mn 2p and Ni $2p_{2/3}$ images in Figure 1(b), where the dark region is the YSZ electrolyte. The Ni $2p_{2/3}$ spectrum and the bottom Mn 2p spectrum in the Mn panel, shown in Figure 1(c), confirm the NiO (Ni^{2+}) and MnO_2 (Mn^{4+}) initial chemical state of the electrodes[10,11]. Within our micrometer resolution the Mn 2p and Ni $2p_{2/3}$ maps taken during cell operation, i.e. after switching from O_2 to H_2 or $H_2 + O_2$ ambient, did not reveal further structural changes or mass transport of electrode material promoted in externally-driven cells when applying biases exceeding 1 V[5,6]. It has to be notified that for the H_2 fuel used in the present system, the XPS spectra measured on both electrodes before and during operation of the cell did not evidence presence of any C deposits or other contaminants. In fact, as stated in one of our previous studies[6] C deposition on the electrodes is an issue when using hydrocarbon fuels and is promoted by applying cathodic potentials.

The time-evolution of the oxidation state and local potential of the working Ni anode is exemplified by the Ni $2p_{2/3}$ spectra in Figure 2(a), measured close to the Ni/YSZ interface (three-phase boundary): the most electrochemically active region. Immediately after switching to H_2 or $H_2 + O_2$ the Ni $2p_{2/3}$ spectrum undergoes a rigid energy shift. Since in the initial state the Ni electrode is oxidized, the shift is better evidenced by the Ni^{2+} component that is present in all spectra. The spectra energy shift is a measure of the over-potential resultant from the current flow generated by the hydrogen oxidation that starts on the NiO electrode: this process is anodic so the shift is to higher binding energy (lower kinetic energy). The maximum shift is of the order of 0.75 eV for H_2 and 0.85 eV for $H_2 + O_2$ ambient. The spectral shifts also show that in the case of $H_2 + O_2$ ambient a constant potential (current) after about 8–10 minutes is reached, whereas in H_2 ambient there is a slight backward shift by about 0.15 eV at longer reaction times. This is an indication of the decrease of the current level, that can be attributed to progressive reduction of the MnO_2 cathode to MnO, as evidenced by the top Mn spectrum in Figure 1(c) measured in pure H_2 ambient. As discussed more extensively in the SI, for our cell configuration and electrical connections, the overpotential shifts are observed only at the electronically conductive Ni (NiO) anode. The Mn (Mn oxide) electrode,

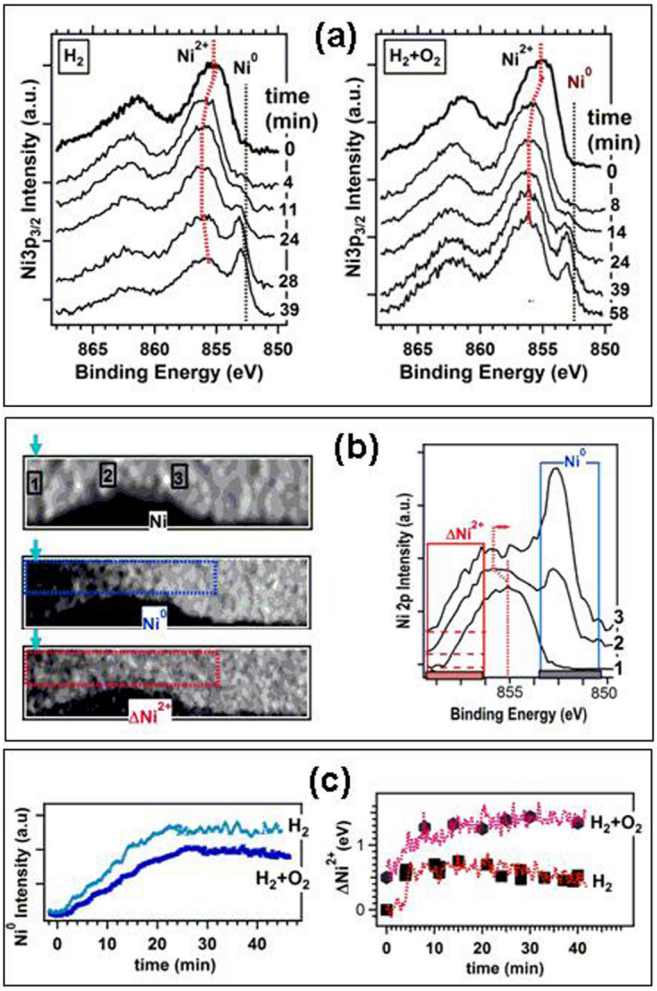

Figure 2 | (a) Evolution of μ-PES Ni 2p spectra after switching from O_2 to H_2 (left panel) or H_2 + O_2 (right panel) ambient keeping 10^{-5} mbar pressure (650°C). (b) Left: (top) 64 × 16 μm² (256 × 64 pixels) Ni 2p map where each vertical scan corresponds to 32 sec; (bottom) Ni 2p spectra extracted from selected locations 1, 2 and 3 indicated in the Ni $2p_{2/3}$ map, representing the Ni initial, transient and final chemical states after switching to H_2 ambient (650°C). The blue and red boxes indicate the energy windows outlining the evolution of the Ni^0 and Ni^{2+} components, which are used for construction of the Ni^0 'reduction' map and the Ni^{2+} map tracing the current-induced shift: Right (top) Ni^0 'reduction map' and reduction rate plot, elucidated from the averaged intensity over the indicated area in map; (bottom) Ni^{2+} map constructed by normalization of the Ni^{2+} intensity contrast to outline the current-induced shift. The area used for elucidating the shift is indicated. (c) Plots of the current-induced shifts after switching to H_2 (left) and H_2 + O_2 (right) ambient (650°C). The red lines show the results obtained from the intensity profiles of the corresponding normalized Ni^{2+} maps. The black squares are the results obtained from the μ-PES Ni 2p spectra.

electronically grounded through the Au matrix, is electrochemically reacting due to ionic conductivity and exhibits a homogeneous potential regardless of the sampled position[12]. That is why the Mn 2p spectra do not undergo any over-potential shift, but only a line-shape change due to partial reduction to MnO. For this reason further-on we consider only the evolution of the Ni electrode.

The Ni $2p_{2/3}$ spectra in Figure 2(a) also show that the on-going electrochemical reaction is accompanied by progressive partial reduction of the NiO electrode, evidenced by the growth of a metallic Ni^0 component at the expense of the Ni^{2+} one, until a steady state is reached after ~25–30 minutes. It should be notified that in H_2 + O_2 ambient the weight of the Ni^0 component reaches a maximum and slightly decreased in advanced reaction stages (see the spectrum taken at 58 minutes). The reason is that in this case H_2 oxidation and anodic oxidation concur at the same time (for details, see Section 2 of SI).

The current-induced spectral shift and the progressing NiO reduction as a function of the reaction time can be monitored with higher temporal resolution using the imaging mode, i.e. starting the Ni 2p maps of the electrode in the vicinity of the electrolyte and switching to H_2 or H_2 + O_2 ambient after several scans. Using the Ni $2p_{3/2}$ energy window covering both oxide and metal components the maps encode the initial state and the evolution after starting the reaction. The duration of each vertical scan determines the time resolution, which in the present study is 32 sec – good compromise for getting sufficient signal to follow the growth of the metallic Ni^0 component at the expense of the oxide Ni^{2+} one and the over-potential shift. The top Ni image in Figure 2(b) shows the contrast for the selected Ni $2p_{3/2}$ energy window; since the total intensity of emitted photoelectrons remains practically constant, only features due to the sample grainy structure are visible. The right panel shows the reconstructed Ni $2p_{2/3}$ spectra from the three typical locations indicated in the Ni map, representing initial oxide state before switching to H_2 ambient,

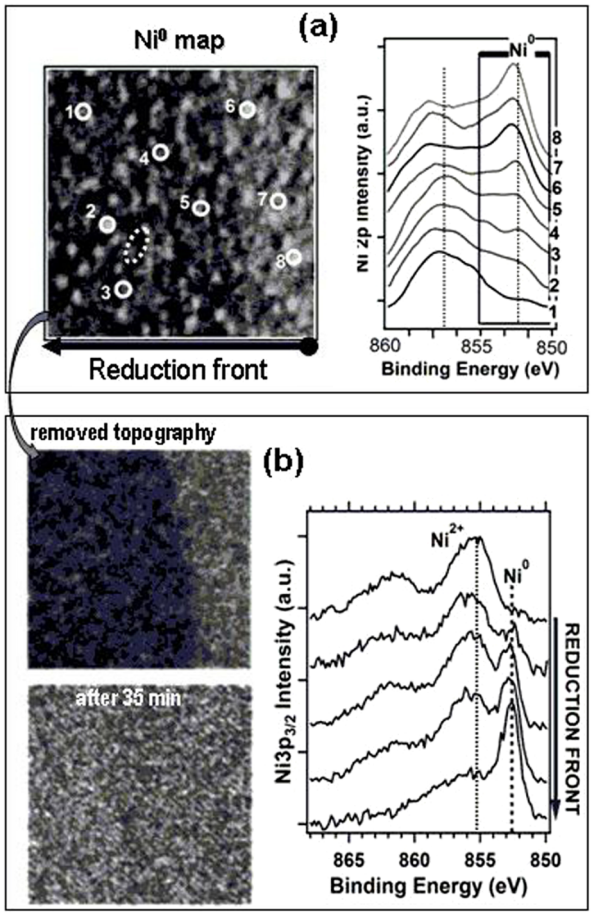

Figure 3 | (a) 32 × 32 μm² Ni^0 map (left) and Ni 2p spectra (right) taken in indicated locations immediately after switching from O_2 10^{-5} mbar to H_2 1 mbar (650°C). (b) Chemical maps obtained after removing the topography contrast from (a) (top) and taken after 35 minutes (bottom) (650°C). The topography contrast was removed by dividing the Ni^0 image to the background image[13]. The μ-PES spectra shown in the right panel were measured at regular time intervals in a micro-spot within the region indicated by the ellipse in Ni^0 map in (a). The dashed lines in the spectra panels indicate the position of the Ni 2p components and potential-induced shifts.

and the states after different reaction (scanning) times. The spectra confirm both the advancement of reduction and the over-potential shift, better monitored by the oxide Ni^{2+} component. By selecting the proper channels covering the selected energy windows, indicated in the spectra panel, we obtained the Ni^0 and ΔNi^{2+} maps. The increase of the brightness level in the Ni^0 map outlines the growth of the metallic Ni^0 component with time, which measures the reduction rate, whereas the increasing brighteness in the ΔNi^{2+} map reflects the increasing fraction of the Ni^{2+} signal within the selected energy window as a result of the overpotential-related energy shift. From these two maps we were able to quantify the transient dynamics relevant to the partial NiO reduction and current generation. The plots for the H_2 and $H_2 + O_2$ ambients, extracted from the image contrast of the Ni^0 and ΔNi^{2+} maps averaging the signal over the indicated selected area, are shown in Figure 2(c). The Ni^0 intesity vs time plots show that a steady partially reduced Ni state is attained in about 20–25 and 25–30 minutes after switching to H_2 and $H_2 + O_2$ ambients, respectively, which is in agreement with the μ-PES results in Figure 2(a). The ΔNi^{2+} plots, normalized to the maximum current-induced spectral shifts measured from the spectra also show the same trend measured from the spectra in Figure 2(a) (denoted by markers). However, it is obvious that using imaging mode the statistics is much better. The results reported in Figure 2 have further been confirmed with a series of cognate gas switching experiments from 10^{-5} mbar O_2 to 1 mbar H_2, detailed in Section 4 of SI.

Using higher H_2 pressures we also investigated the propagation of the reduction front, ignited at the interface, inside the electrode, Figure 3(a) displays a map of the Ni^0 energy window (defined in the spectra panel on the right) measured inside the electrode at a distance of 60 μm from the interface. The map appears brighter on the right hand side, which indicates the growth of Ni^0 component due to the penetration of the reduction front. The reconstructed spectra from different locations 1–8, indicated in the map, confirm that the right part is in a more advanced reduction stage. Close inspection of the spectra extracted from the different positions reveals the lateral variation in the oxidation state and the potential-induced shifts. By removing the topography contrast the 'chemical' maps, shown in Figure 3(b), can be obtained. The top one outlines clearly the boundary of the reaction front and the bottom one, taken after 35 minutes, shows no chemical contrast, since the whole mapped region has been reduced. The propagation of the reduction wave and advancement of reduction with time was further evidenced by the consecutive μ-PES measured in the location indicated by the dashed ellipse in the Ni^0 map in Figure 3(a). The bottom spectrum, taken after 35 minutes, confirms the almost complete Ni reduction at this higher H_2 pressure.

Discussion

The SPEM images taken within the energy windows of the Ni 2p and Mn 2p photoelectron emission and the evolution of the Ni 2p and Mn 2p spectra measured in selected location on the electrodes of the Ni|YSZ|Mn single self-driven cell, demonstrate how spontaneous electrochemical processes can be followed in terms of local overvoltage rise and evolution of the electrode oxidation state. The spectral transients recorded under operating cell conditions, resulting in generation of electric current, encode both the time-dependent electrochemical kinetics through spectral energy shifts and the electrode oxidation states resuting from electrochemical or/and chemical processes. The electrochemical (ec) and chemical (c) reactions taking place on the electrodes in both H_2 and $H_2 + O_2$ reaction ambient under our experimental conditions, summarized in Figure 4(a) and (b), are in full accordance with the obtained results. No reaction occurs on the MnO_2 and NiO electrodes kept in O_2 atmosphere, the initial state before switching to operation (H_2 or $H_2 + O_2$) ambient (see SI). The electrochemical oxidation of H_2 at the NiO anode and the reduction of the Mn-oxide cathode is simulating battery and ultracapacitor behavior, whereas the O_2 reduction is simulating solid-oxide fuel-cell behavior.

In both H_2 and $H_2 + O_2$ ambients the electrochemical H_2 oxidation catalysed at the NiO anode is accompanied with chemical reduction of NiO by H_2. Since on the anode the chemical reduction competes with the electrochemical anodic oxidation, it results in partial NiO reduction under low reactant gas pressure (10^{-5} mbar) conditions. Apparently, the reduction is more advanced in pure H_2 ambient, as evidenced by the evolution of the Ni 2p spectra in Figure 2. The recorded spectral transients after switching to

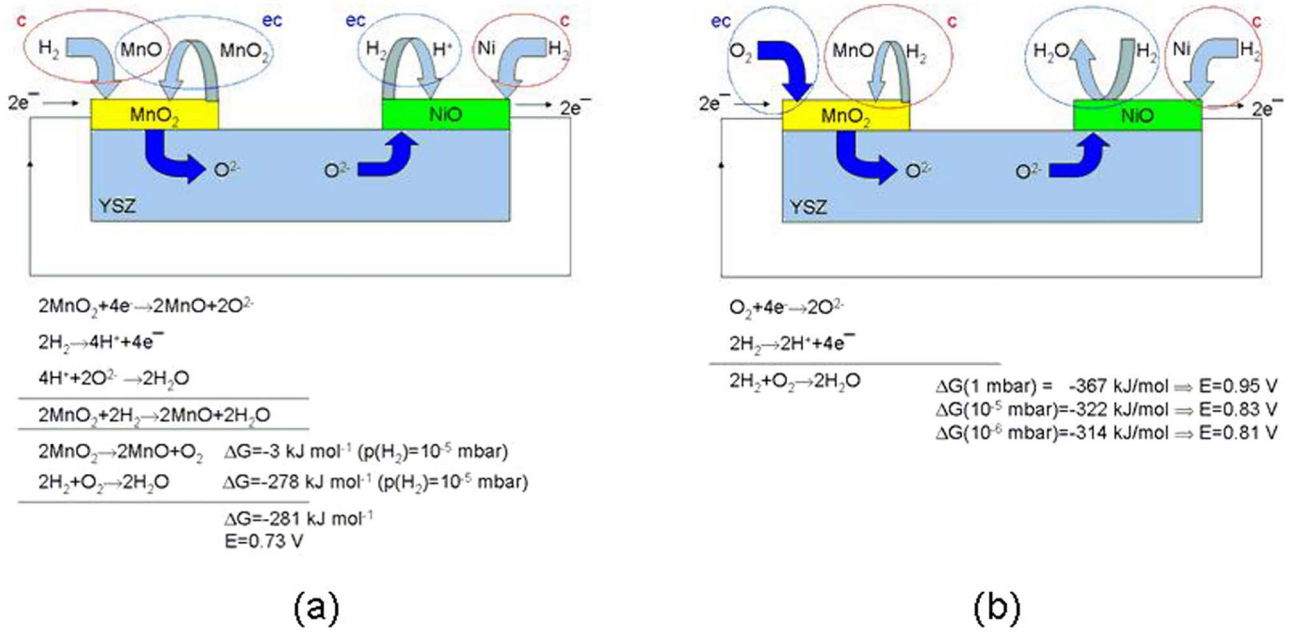

Figure 4 | (a) Reaction scheme for a MnO_2/YSZ/NiO cell in H_2 and corresponding thermodynamics for 10^{-5} mbar H_2 (c: chemical, ec: electrochemical). (b) Reaction scheme for a MnO_2/YSZ/NiO cell in $H_2 + O_2$ mixture and corresponding thermodynamics for 10^{-6}, 10^{-5} and 1 mbar; chemical reduction reactions of electrodic materials, possible in the gas mixture, are also shown. More extensive explanations can be found in Section 2 of SI.

operation conditions, represent the time-dependent electrochemical kinetics through overvoltage-induced spectral shifts, recorded both in the spectral and imaging modes. Note the very good agreement between the numbers predicted for the potential generated from the electrochemical reaction and the one measured from the spectral shifts and reported in Figure 2(c). Another very important finding is that there is no correlation between the oxidation state of the anode resulting from the chemical reaction (reduction by H_2 in the present system) and the potential generated from the electrochemical reaction: it is evident comparing the reduction rate and potential changes manifested by the plots in Figure 2(c). The results show that the potential reaches a maximum within 5–10 minutes whereas the steady state reduction state is attained after 25–30 minutes. This can be attributed to the fact that the steady state is determined by the competition between chemical reduction rate and anodic oxidation rate.

The MnO_2 cathode can undergo electrochemical reduction to MnO while catalyzing O_2 reduction: the O^{2-} ions, released to YSZ, move to the anode to produce water reacting with H^+. MnO_2 can also undergo reduction in H_2 ambient, but the MnO is the stable form in H_2 environment, as confirmed by our measurements and detailed in Section 2 of the Supplementary Information (SI) and references therein contained.

These first SPEM results obtained following in-situ the evolution of chemical state and local potential at the electrodes of a Ni|YSZ|Mn single self-driven cell have shed light on competing electrochemical and chemical processes occurring in real electrochemical devices generating electrical current. They demonstrate the great potential of the advanced experimental approach we used, to gain insight into electrochemical and chemical processes taking place in energy conversion systems, which could guide the design of next-generation devices with improved performance.

Methods

The experiments were performed with the SPEM operated at Elettra-Sincrotrone Trieste[14]. The SPEM imaging mode can map the elemental, chemical state and charge distribution by collecting photoelectrons emitted within a selected kinetic energy window, covered by the 48 channels of the detector, while raster-scanning the specimen with respect to the microprobe. Each detector channel measures electrons with specific kinetic energy, which provides 48 images and also allows the reconstruction of the spectrum corresponding to this window from a selected micro-area. The better spectral resolution (0.18 eV) of the second microspot PES mode (μ-PES) provides more precise information for the chemical state and local potential with lateral resolution down to 100 nm[15]. Electrochemical measurements were made with a PAR potentiostat.

1. Corcoran, C. J. *et al.* Application of XPS to study electrocatalysts for fuel cells. *J. Power Sources* **195**, 7856–7879 (2010).
2. Zhang, C. *et al.* Measuring fundamental properties in operating solid oxide electrochemical cells by using *in situ* X-ray photoelectron spectroscopy. *Nature Materials* **9**, 944–949 (2010).
3. Zhang, C. *et al.* Multielement Activity Mapping and Potential Mapping in Solid Oxide Electrochemical Cells through the use of *operando* XPS. *ACS Catal.* **2**, 2297−2304 (2012).
4. Bozzini, B. *et al.* Soft X-ray imaging and spectromicroscopy: new insights in chemical state and morphology of key components in operating fuel cells. *Chemistry-A European Journal* **18**, 10196–10210 (2012).
5. Bozzini, B. *et al.* In-situ X-ray spectromicroscopy investigation of the material stability of SOFC metal interconnects in operating electrochemical cell. *ChemSusChem* **4**, 1099–1103 (2011).
6. Bozzini, B. *et al.* Micro scale evolution of surface chemistry and morphology of the key components in operating hydrocarbon-fuelled SOFC. *J. Phys. Chem. C* **116**, 23188–23193 (2012).
7. Bozzini, B. *et al.* In situ electrochemical X-ray spectromicroscopy investigation of the reduction/reoxidation dynamics of Ni-Cu Solid Oxide Fuel Cell anodic material in contact with a Cr interconnect in 2×10^{-6} mbar O_2. *J. Phys. Chem. C* **116**, 7243–7248 (2012).
8. El Galbaly, F., McCarty, K. F., Bluhm, H. & McDaniel, A. H. Oxidation stages of Ni electrodes in solid oxide fuel cell environments. *Phys. Chem.Chem. Phys* **15**, 8334–8341 (2013).
9. Bozzini, B. *et al.* In situ photoelectron microspectroscopy during the operation of a single-chamber SOFC. *Electrochem. Comm.* **24**, 104–107 (2012).
10. Biesinger, M. C. *et al.* X-ray photoelectron spectroscopic chemical state quantification of mixed nickel metal, oxide and hydroxide systems. *Surf. Interface Anal.* **42**, 324–332 (2009).
11. Biesinger, M. C. *et al.* Resolving surface chemical states in XPS analysis of first row transition metals, oxides and hydroxides: Cr, Mn, Fe, Co and Ni. *Appl. Surf. Sci.* **257**, 2717–2730 (2011).
12. Benaissa, M., José-Yacamán, M., Xiao, T. D. & Strutt, P. R. Microstructural study of hollandite-type MnO_2 nano-fibers. *Appl. Phys. Lett.* **70**, 2120–2122 (1997).
13. Günther, S., Kolmakov, A., Kovac, J. & Kiskinova, M. Artefact formation in scanning photoelectron emission microscopy. *Ultramicroscopy* **75**, 35–51 (1998).
14. http://www.elettra.trieste.it/elettra-beamlines/escamicroscopy.html date of access: August 9th, 2013
15. Gregoratti, L. *et al.* 48-Channel electron detector for photoemission spectroscopy and microscopy. *Rev. Scient. Instr.* **75**, 64–69 (2004).

Author contributions

B.B. and M.K. have contributed equally in elaborating the data, writing the main manuscript and preparing the figures. M.A. and L.G. set up and run the ESCAmicroscopy beamline and contributed to the quantitative elaboration of the XPS spectra and SPEM images. M.A., B.B. and L.G. performed the beamtime. B.B. designed and fabricated the electrochemical cells, in collaboration with the TASC Laboratory of Elettra.

Additional information

Supplementary information accompanies this paper at http://www.nature.com/scientificreports

Competing financial interests: The authors declare no competing financial interests.

How to cite this article: Bozzini, B., Amati, M., Gregoratti, L. & Kiskinova, M. In-situ Photoelectron Microspectroscopy and Imaging of Electrochemical Processes at the Electrodes of a Self-driven Cell. *Sci. Rep.* **3**, 2848; DOI:10.1038/srep02848 (2013).